



Research article

Hypergraph representation of multimodal brain networks for patients with end-stage renal disease associated with mild cognitive impairment

Zhengtao Xi^{1,†}, Tongqiang Liu^{2,†}, Haifeng Shi³ and Zhuqing Jiao^{4,*}

¹ School of Microelectronics and Control Engineering, Changzhou University, Changzhou 213164, China

² Department of Nephrology, The Affiliated Changzhou No.2 People's Hospital of Nanjing Medical University, Changzhou 213003, China

³ Department of Radiology, The Affiliated Changzhou No.2 People's Hospital of Nanjing Medical University, Changzhou 213003, China

⁴ School of Computer Science and Artificial Intelligence, Changzhou University, Changzhou 213164, China

† Zhengtao Xi and Tongqiang Liu should be regarded as joint first authors.

* **Correspondence:** Email: jzq@cczu.edu.cn.

Abstract: The structure and function of brain networks (BN) may be altered in patients with end-stage renal disease (ESRD). However, there are relatively few attentions on ESRD associated with mild cognitive impairment (ESRDaMCI). Most studies focus on the pairwise relationships between brain regions, without taking into account the complementary information of functional connectivity (FC) and structural connectivity (SC). To address the problem, a hypergraph representation method is proposed to construct a multimodal BN for ESRDaMCI. First, the activity of nodes is determined by connection features extracted from functional magnetic resonance imaging (fMRI) (i.e., FC), and the presence of edges is determined by physical connections of nerve fibers extracted from diffusion kurtosis imaging (DKI) (i.e., SC). Then, the connection features are generated through bilinear pooling and transformed into an optimization model. Next, a hypergraph is constructed according to the generated node representation and connection features, and the node degree and edge degree of the hypergraph are calculated to obtain the hypergraph manifold regularization (HMR) term. The HMR and L_1 norm regularization terms are introduced into the optimization model to achieve the final hypergraph representation of multimodal BN (HRMBN). Experimental results show that the

classification performance of HRMBN is significantly better than that of several state-of-the-art multimodal BN construction methods. Its best classification accuracy is 91.0891%, at least 4.3452% higher than that of other methods, verifying the effectiveness of our method. The HRMBN not only achieves better results in ESRDaMCI classification, but also identifies the discriminative brain regions of ESRDaMCI, which provides a reference for the auxiliary diagnosis of ESRD.

Keywords: end-stage renal disease; mild cognitive impairment; multimodal brain network; hypergraph representation; classification

1. Introduction

End-stage renal disease (ESRD) is usually accompanied by renal failure, central nervous system abnormalities and multiple organ dysfunction [1]. It may lead to cognitive dysfunction, including abnormal cognitive control, memory impairment and emotional impairment [2]. Cognitive impairment is a common comorbidity in ESRD cases, especially for patients receiving hemodialysis (HD). The impairment of cognitive function is more common in orientation, attention, and executive function [3]. About 30–60% of ESRD patients will develop mild cognitive impairment (MCI) when receiving HD treatment [4]. MCI patients have a high risk of developing dementia, which may significantly reduce the survival rate and prognosis. After cognitive training and rehabilitation treatment, the development of dementia in MCI patients may be delayed, and some may even return to a normal state [5]. However, the exact neuropathological mechanism of ESRD associated with MCI (ESRDaMCI) is still unclear, and hinders the development of effective treatment. Therefore, the diagnosis of neuroimaging changes in ESRD patients with MCI is critical for effective treatment and prognosis improvement in these patients.

In recent years, multimodal neuroimaging techniques, including structural magnetic resonance imaging (sMRI) [6], fluorodeoxyglucose positron emission tomography (FDG-PET) [7], arterial spin labeling (ASL) [8], and functional magnetic resonance imaging (fMRI) [9], diffusion tensor imaging (DTI) [10] and diffusion kurtosis imaging (DKI) [11], have developed rapidly. Researchers can understand the pathophysiology of brain diseases in different aspects, such as pathological marker deposition, structural connectivity (SC) and functional connectivity (FC). These provide a valuable tool for the studies of potential imaging biomarkers of ESRD associated with neurological complications. Previous studies on voxel-based morphometrics, surface-based morphometrics, and DTI, revealed gray matter volume defects and reduced cortical thickness in ESRD patients, as well as reduced white matter integrity [12]. The Alzheimer's Disease Imaging Initiative reported the possibility of DTI as a biomarker of cognitive impairment [13], whereas, DTI could not accurately reflect the changes of brain tissue microstructure because it could not quantify non-Gaussian diffusion. DKI overcomes these limitations and provides a new way to analyze the microstructure of gray matter and white matter. It has been applied to the studies of nervous systems, including normal brain tissue, cerebral infarction [14], brain trauma [15], glioma [16], and Alzheimer's disease [17], etc.

Great deals of attention have been paid to studying the mechanisms of some brain disorders, such as epilepsy [18], schizophrenia [19], Alzheimer's disease [20], and ESRD-related neurological complications [21]. Brain networks (BN) provide powerful representations on the interaction patterns between various brain regions. Nodes in BN represent brain regions divided by physiological templates,

and edges represent interactions between regions extracted from noninvasive imaging techniques. Edges can be classified as FC and SC. FC estimates the consistency of brain activity between different brain regions, which is usually calculated from time series extracted from fMRI or electroencephalogram (EEG) signals. SC describes the physical connection of nerve fibers between brain regions, which can be directly obtained by calculating the number of fiber tracts (FN) in DKI. Many computational models, including sparse learn-based models [22] or graph-theoretic metrics [23], have been applied to search for potential biomarkers from FC or SC for diagnosing brain diseases. Traditional BNs simply takes into account the interactions between pairwise brain regions. This can result in the omission of serviceable information in higher-order relationships between brain regions (that is, broader nodal interactions between more than two brain regions) that are essential for understanding the pathological basis of brain diseases.

Some new methods have been developed fusing FC and SC for BN analysis. Yu et al. [24] described the complex interaction between multiple nodes as hypergraphs. Ji et al. [25] constructed a hypergraph manifold regularization (HMR) framework for brain functional networks. Diffusion processes have been used to analyze multimodal data [26], providing some general learning frameworks. FC provides information about brain activity, while SC directs the flow of information. If SC is directly used as the transition matrix, where the weights are predetermined and cannot solve the classification task. While SC may be helpful in determining interaction links between nodes, link weights between nodes are broadly correlated and complex. The joint feature representation obtained through diffusion is yet in the node level, which is different from the global level connections of BN [27].

In this study, a hypergraph representation method of multimodal BN is proposed. The node representation is optimized by fusing FC and SC to automatically learn interactions between nodes, considering direct and indirect connections. Specifically, firstly, the node feature matrix is constructed according to the time series extracted from fMRI, and the adjacency matrix is constructed according to the number of FN extracted from DKI. On this basis, an attention spread graph is defined to describe the node interaction based on the input node connection graph. It is called the node feature matrix, where the weight (strength) of the node connection can be automatically learned through training. The diffusion process guided by the attention diffusion map (ADM) integrates fMRI and DKI datasets to generate corresponding node representations. Then, the connection features for classification are generated by bilinear pooling and transformed into an optimization model. Finally, the hypergraph is constructed according to the generated node representation and connection features. HMR and L_1 norm regularization terms are introduced into the optimization model to obtain the hypergraph representation of multimodal BN (HRMBN) for ESRDaMCI classification.

The major contributions and novelty are as follows. a) A hypergraph representation method is proposed for the first time to integrate fMRI and DKI to construct multimodal BN considering the complementary information of FC and SC of ESRDaMCI; b) It is the first time to construct hypergraphs based on node representations and connection features generated by fMRI and DKI, and the first time to introduce HMR and L_1 norm regularization terms into the optimization model constructed by bilinear attention mechanism; c) More desirable results are obtained in the classification of ESRDaMCI, and the key brain regions are identified, which provided a reference for the clinical research and auxiliary diagnosis of ESRDaMCI.

2. Materials and methods

2.1. Research framework

Figure 1 shows the hypergraph representation framework: (a) Preprocessing fMRI data and DKI data obtained by scanning; (b) Extracting time series from fMRI, and tracing fiber tracts from DKI; (c) Constructing the node feature matrix for time series, and constructing the adjacency matrix for FN obtained from fiber bundle tracking; (d) Constructing an ADM based on node features and adjacency matrix to guide the diffusion process to generate node representation; (e) Using bilinear pooling to generate connection features, which is transformed into an optimization model; (f) Constructing hypergraph based on node representation and connection features, and obtain hypergraph Laplacian matrix; (g) Calculating HMR term by hypergraph Laplacian matrix, and introducing HMR and L_1 norm regularization terms into the optimization model at the same time to acquire the HRMBN; (h) Taking the network edge weights in BN as features for feature selection to obtain discriminative features; (i) Dividing the selected features into a training set and a test set, and using the former to train the classifier, then classifying the later and evaluating its classification performance.

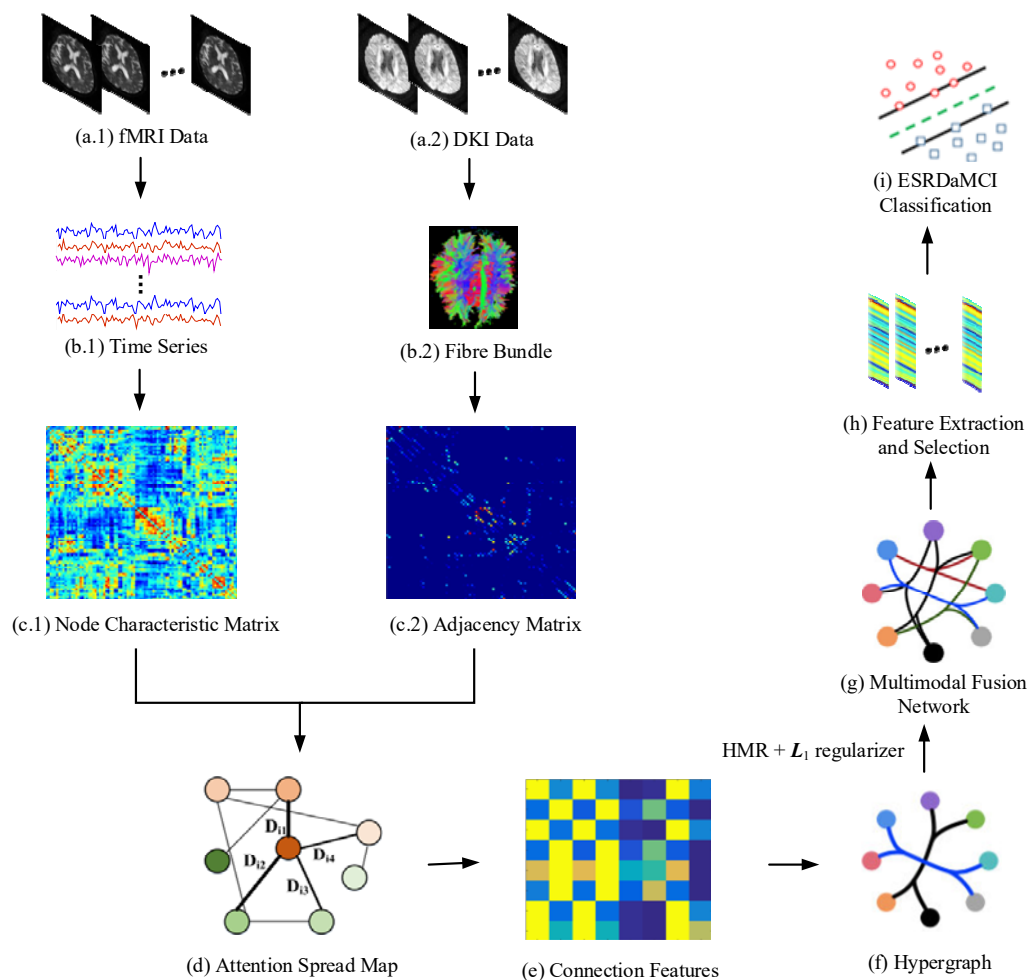


Figure 1. Hypergraph representation framework diagram.

2.2. Data preparation

Fifty-one ESRD patients diagnosed with MCI in Changzhou Second People's Hospital Affiliated to Nanjing Medical University from February 2020 to June 2021 are included in ESRDaMCI group. Their average length of education is (11.25 ± 3.15) years (range, 5–19 years). All of them are right-handed and had no previous cardiovascular disease; No neurological disease; Free from infectious diseases; No diabetes; There are no contraindications of magnetic resonance examination. Meanwhile, thirty-nine healthy volunteers are recruited to the normal group. The average length of education is (9.73 ± 3.85) years (range, 5–19 years). All of them are right-handed; Previously in good health; There are no contraindications of magnetic resonance examination. There are 5 cases in ESRDaMCI group and 3 cases in normal group who are excluded due to excessive head movement. Finally, 51 patients and 39 volunteers are included. This study was approved and supervised by the Ethics Committee of Changzhou Second People's Hospital Affiliated to Nanjing Medical University, with the approval number KY039-01. All subjects voluntarily signed written informed consent.

Montreal Cognitive Assessment (MoCA) includes 11 items that measure multiple cognitive domains, such as memory, language, abstract thinking, executive functioning, visuospatial skills, attention and concentration, computation, and orientation [28]. According to the statistics from Changzhou Second People's Hospital Affiliated to Nanjing Medical University, MoCA has a better completion degree and a higher sensitivity to identify MCI in memory clinic than other cognitive function assessment scales, due to some factors such as patients' short temper and lack of cooperation. Therefore, MoCA is used to evaluate the cognitive function of ESRD patients and normal people. The full score of the MoCA scale is 30 points, with 26 or more as normal, 18–26 as mild, 10–17 as moderate, and less than 10 as severe. The average score of ESRD patients diagnosed with MCI is 21.30 ± 2.75 . Table 1 shows the specific demographic information.

Table 1. Demographic information.

| Item | ESRDaMCI ($n = 51$) | Normal ($n = 39$) | t/χ^2 | P |
|-------------------------------------|-----------------------|---------------------|------------|-------|
| Age ($\bar{x} \pm s$) | 50.05 ± 7.86 | 48.37 ± 6.59 | 1.079 | 0.251 |
| Gender (M/F) | 24/27 | 24/15 | 0.341 | 0.536 |
| Education years ($\bar{x} \pm s$) | 11.25 ± 3.15 | 9.73 ± 3.85 | 0.973 | 0.771 |
| MoCA score ($\bar{x} \pm s$) | 21.30 ± 2.75 | 27.27 ± 1.24 | -13.728 | 0.000 |

Note: ESRDaMCI: ESRD patients diagnosed with MCI; Normal: Normal people; $P < 0.05$ is a statistically significant difference.

In GE Discovery MR 750W 3.0T scanner, A rubber cork was used to fix the head to avoid artifacts caused by head movement during the test. All subjects first underwent conventional MR examination, including T2-weighted (T2WI) and fluid attenuation inversion recovery (FLAIR) sequence T2WI. Two diagnostic imaging physicians ruled out organic brain damage. T1WI high-resolution structural images of the whole brain were acquired by 3D brain volume imaging (3D BRAVO) sequence with repetition time (TR) = 8.2 ms, echo time (TE) = 3.2 ms, layer thickness = 1.2 mm, layer interval = 0 mm, and flip angle = 12° . The matrix size = 256×256 , the field of view (FOV) = $240 \text{ mm} \times 240 \text{ mm}$, the number of scanning layers = 152, and the scanning time = 3 min 57 s.

Single excitation plane echo imaging (SS-EPI) sequence was used for DKI scanning, divided into 30 diffused susceptibility directions, b value = 0, 1000, 2000 s/mm^2 , TR = 6500 ms, TE = 95.8 ms, FOV = 240.0 mm \times 240.0 mm, matrix size = 128 \times 128, layer thickness = 3.6 mm, the layer spacing = 0, the excitation times = 2, the number of scanning layers = 30, and the scanning time = 14 min 43 s. Gradient-echo plane echo imaging (GRE-EPI) sequence was used for fMRI scanning. The machine scanning parameters are as follows: Repetition time (TR) = 2000 ms, echo time (TE) = 40 ms, field of view (FOV) = 24 cm, flip angle (FA) = 90°, matrix size = 64 \times 64, the layer thickness = 6 mm. Complete the MoCA evaluation before scanning.

The DKI data is preprocessed in FSL_5.0 and PANDA of Diffusion Toolkit [29]. Complete the following steps: 1) Format conversion: Transform the original data of DICOM format for 4 DNIFTI format using MRICRON “dcm2nii” in software toolkit; 2) eddy current correction: Remove data with large head movement to ensure the consistency of data; 3) Gradient correction and smooth noise reduction: Correct for subtle differences between brain structures and reduce spatial noise; 4) Acquisition of brain mask image: Extract b_0 image, and then obtain the corresponding mask through the b_0 image; 5) Calculating tensor, Fractional Anisotropy index (FA), Mean Diffusivity (MD) equivalent; 6) Resampling: Register the image to the standard space of Montreal Neurological Institute (MNI); 7) Gaussian smoothing and transforming the Automated Labeling (AAL) template in MNI space into the node in the brain structural network in individual space; 8) White matter fiber tract tracking: Use deterministic fiber tract tracking algorithm to calculate FN and Fractional Anisotropy (FA) and other indicators between brain regions.

The fMRI data is preprocessed in SPM8 and DPARSF of Matlab 2012b platform [30]. The specific steps are as follows: 1) Format conversion: Use DICOM Import of SPM8 to convert DICOM format into NIFTI format; 2) Slice Timing: Delete the first 10 time points and use the remaining 230 time series for subsequent processing; 3) Realign and normalize: Use the rigid registration for head correction, and normalize the fMRI images to MNI space and then standardize (Bounding Box: [-90, -126, -72; 90, 90, 108], Voxel Size: [3 3 3]). 4) Smooth: Use full-width-at-half-maximum to smooth the Gaussian kernel; 5) Detrend; 6) Band pass filtering: Set frequency range from 0.01 to 0.08 Hz; 7) Region partition: Divide a brain into 90 brain regions using AAL standard partition template, and extract the time series for the convenience of subsequent research.

2.3. Definition of nodes and edges

Given a BN $G(V, E)$, $V = \{v_1, v_2, \dots, v_n\}$ represents a group of nodes (brain regions), $E = \{e_{ij}\}$ ($i, j = 1, 2, \dots, n$) represents a set of edges (connections between nodes). Suppose $F = \{F_1, F_2, \dots, F_n\}$, $F_i \in \mathbf{R}^n$ is the feature set of nodes, and $S \in \mathbf{R}^{n \times n}$ is the corresponding adjacency matrix. F represents a node feature matrix consisting of *Pearson's* correlation coefficients between fMRI time series. S represents a FN adjacency matrix, and FN can represent the strength of SC in BN. When the FN between two nodes is more than 3, there is a connection [31]. The adjacency matrix of FN is normalized by Minmax to improve the speed and accuracy of iterative solution and eliminate the dimensional difference of variables.

The diffusion process is randomly transferred on a graph, and the transition matrix can be expressed as:

$$P = \{p_{ij}\} \quad (i, j = 1, 2, \dots, n) \quad (1)$$

where p_{ij} represents the predetermined transition probability of moving from one node to another in a one-step diffusion.

In the scenario of BN analysis, the diffusion process can be affected by the node characteristics defined by FC. Adding attention mechanism can solve this concern [32]. The attention diffusion process (ADP) can generate node representations by considering both node features and SC, thus naturally fusing SC and FC.

The node interaction is computationally represented by using the node feature matrix F and the adjacency matrix S . Specifically, the connections of nodes are determined by SC, and the weight of node interactions may be influenced by node features. This is due to the realization that the SC of the brain is fixed, whereas the FC of the brain is not fixed and depends on different nodal interactions between different brain systems. In this way, the weight of interaction strength between node i and node j is denoted as:

$$c_{ij} = f(W_c \cdot (W_\alpha F_i \parallel W_\alpha F_j) + b_c) \quad (2)$$

where \parallel means to concatenate two vectors, $W_c \in \mathbf{R}^{1 \times 2d}$ is a trainable weights matrix; $W_\alpha \in \mathbf{R}^{d \times n}$ is a learnable linear projection matrix to improve the expression ability of the original features. b_c is the bias term, a constant, and it learns with the whole model; f is an activation function.

Since C is not symmetric, the influence is directional and can reflect the influence degree of node i on node j . The weight matrix C is normalized to construct the attention spread map D for consistency comparison between different nodes. D is formulated as:

$$D_{ij} = \text{softmax}(c_{ij}) = \frac{\exp(c_{ij})}{\sum_{k \in N_i} \exp(c_{ik})} \quad (3)$$

where N_i represents the set of adjacent elements of element i of the adjacency matrix S .

Only N_i is considered for normalization to reflect SC between brain regions. If multistep diffusion is performed, it is no longer reasonable to use the power series of the attention spread graph D . This is because the attention mechanism changes with diffusion, reflecting the dynamic characteristics of BN. Therefore, an independent attention mechanism is applied to calculate the weight of the diffusion process and normalize it:

$$D_{ij}^t = \frac{\exp(f(W_c^t \cdot (W_\alpha^t F_i \parallel W_\alpha^t F_j) + b_c^t))}{\sum_{k \in N_i^t} \exp(f(W_c^t \cdot (W_\alpha^t F_i \parallel W_\alpha^t F_k) + b_c^t))} \quad (4)$$

where N_i^t represents the set of adjacent elements of the element i of the adjacency matrix S in the t -step diffusion, namely $S^t = S \underset{t}{\times} S$.

Nodes of a multimodal BN can be represented as $Z^t = \{Z_1^t, Z_2^t, \dots, Z_n^t\}$, and after the t -step ADP $Z_i^t \in \mathbf{R}^d$ can be formulated as:

$$Z_i^t = \sum_{k \in N_i} D_{ik}^t W_\alpha^t F_k \quad (5)$$

where $D^t \in \mathbf{R}^{n \times n}$ is the ADM in the t -step diffusion, representing node interactions in t -step diffusion. The advantage of multistep diffusion is that it can capture potential connections between nodes, which is sensitive to the identification of brain diseases. N_i represents the set of neighboring nodes of node i

according to the adjacency matrix \mathcal{S} . $\mathbf{W}_\alpha \in \mathbf{R}^{d \times n}$ learns along with the entire model. Since the training process is guided by the label (patient is 1, normal is -1), the \mathbf{W}_α learning matrix in Eq (5) can improve the recognition ability of the original features.

Node representation is enhanced by fusing the functionality and structure, as well as leveraging other node information. Nevertheless, these are still node-level features that reflect only local information. Thus, we need to generate connection features from the enhanced node representations. Bilinear pooling is used to extract the node representation information in the entire network to generate connection features:

$$B_{ij}^t = \mathbf{Z}_i^{tT} \cdot \mathbf{Z}_j^t \quad (6)$$

where $\mathbf{B}^t \in \mathbf{R}^{n \times n}$ is bilinear feature. There are at least two benefits to using these features. First, these features can be viewed as connecting features that generate an overall representation of BN. Second, these features can improve classification sensitivity [33].

After centralization and standardization of B_{ij}^t , the BN in the t -step diffusion is expressed as $\mathbf{B}^t = \mathbf{Z}^{tT} \cdot \mathbf{Z}^t$, which is transformed into the optimized form as follows:

$$\min_{\mathbf{B}^t} \left\| \mathbf{B}^t - \mathbf{Z}^{tT} \cdot \mathbf{Z}^t \right\|_F^2 \quad (7)$$

2.4. Introduction of regular term

For the constructed BN, a hypergraph $\mathbf{G} (\mathbf{V}, \mathbf{E}, \mathbf{W})$ can describe the attribute relations between the BN. The set of nodes is denoted as \mathbf{V} , the set of hyperedges is denoted as \mathbf{E} , and the set of weights of each hyperedge is denoted as \mathbf{W} . In hypergraph \mathbf{G} , the node of each BN corresponds to node $v \in \mathbf{V}$ in the hypergraph, and each hyperedge $e \in \mathbf{E}$ contains more than two nodes to represent the simultaneous interaction of multiple BN nodes.

Let $\mathbf{H} \in \mathbf{R}^{|\mathbf{V}| \times |\mathbf{E}|}$ be the point-edge incidence matrix of hypergraph \mathbf{G} , the values of matrix elements are defined as follows.

$$h(v, e) = \begin{cases} 1, & v \in e \\ 0, & v \notin e \end{cases} \quad (8)$$

where $v \in \mathbf{V}$ is a node of hypergraph \mathbf{G} , and $e \in \mathbf{E}$ is a hyperedge of hypergraph \mathbf{G} .

In the incidence matrix \mathbf{H} , the node degree $d(v_i)$ of each node and the edge degree $\delta(e_i)$ of each hyperedge are respectively expressed as:

$$d(v_i) = \sum_{e_i \in \mathbf{E}} w(e_i) h(v_i, e_i), \quad i = 1, \dots, m \quad (9)$$

$$\delta(e_i) = \sum_{v_i \in \mathbf{V}} h(v_i, e_i), \quad i = 1, \dots, m \quad (10)$$

where e_i is the i -th hyperedge, $w(e_i)$ is the weight of the hyperedge, v_i is the i -th node, m denotes the number of hyperedges.

Laplacian matrix is often used in the matrix representation of graphs because it can reflect the intrinsic geometric structure of graphs. The Laplacian matrix of hypergraph can better reflect the higher-order relationship between nodes. It is expressed as

$$\mathbf{L} = \mathbf{D}_v - \boldsymbol{\Theta} \quad (11)$$

where $\boldsymbol{\Theta} = \mathbf{H}\mathbf{W}\mathbf{D}_e^{-1}\mathbf{H}^T$ is the adjacency matrix of the hypergraph, \mathbf{D}_v is the node degree matrix with diagonal elements $d(v_i)$, and \mathbf{D}_e is the hyperedge degree matrix with diagonal elements $\delta(e_i)$.

The standardized Laplacian matrix of a hypergraph is deduced and calculated according to the calculation method of the Laplacian matrix of a simple graph, as shown in Eq (12):

$$\mathbf{L}^h = \mathbf{I} - \mathbf{D}_v^{-\frac{1}{2}} \mathbf{H}\mathbf{W}\mathbf{D}_e^{-1} \mathbf{H}^T \mathbf{D}_v^{\frac{1}{2}} \quad (12)$$

where \mathbf{L}^h is the normalized Laplacian matrix of the hypergraph and \mathbf{I} is the identity matrix. \mathbf{D}_v is the hypergraph node degree matrix, \mathbf{D}_e is the hypergraph hyperedge degree matrix, \mathbf{W} is the diagonal matrix with hyperedge weights, and $\mathbf{H} \in \mathbf{R}^{|\mathcal{V}| \times |\mathcal{E}|}$ is the point-edge incidence matrix of the hypergraph \mathbf{G} .

Referring to the research of Shao et al. [34], the K-Nearest Neighbor (KNN) algorithm is adopted to construct the hypergraph according to the connection features generated by Eq (7), and the node degree and edge degree of the hypergraph are calculated, so as to obtain the regularization term of the hypergraph manifold, and the L_1 norm regularization term is added. Inspired by Huang et al. [32], the ADP is combined with bilinear pooling to take FC as the node. Finally, the multimodal BN is constructed with SC as edges to obtain a HRMBN. The objective function of this method is as follows:

$$\min_{\mathbf{B}^t} \left\| \mathbf{B}^t - \mathbf{Z}^{tT} \cdot \mathbf{Z}^t \right\|_F^2 + \lambda \left\| \mathbf{B}^t \right\|_1 + \beta \operatorname{tr} \left(\mathbf{B}^{tT} \mathbf{L}^h \mathbf{B}^t \right) \quad (13)$$

where \mathbf{B}^t is the hypergraph representation of multimodal in the diffusion at t -step, λ and β represent the regularization parameters of the L_1 norm regularization term and the hypergraph manifold regularization term, respectively, and \mathbf{L}^h is the normalized Laplacian matrix of the hypergraph.

2.5. Feature extraction, selection and classification

After constructing multimodal BN, we determine the features to be used for classification. Two methods are commonly used to identify cognitive impairment. One is to extract features based on some graph metrics, such as local clustering coefficients. The other is to directly take network edge weights as features [35]. This study adopts the second method, which can reduce the impact of the difference of extracted features on the verification of BN itself. The simplest t -test method is used to select features to avoid the confounding effect of feature extraction.

Support vector machine (SVM) has good generalization performance [36]. It uses kernel function to map samples to high-dimensional space during classification, thus simplifying linearly separable problems in high-dimensional space. Linear kernel SVM, with the advantages of easy comparison of experimental results, has been extensively used in small-sample classification problems. Therefore, SVM is selected for this study with only 90 subjects. The discriminative features are selected by t -test, and then SVM is trained to identify patients by using the selected features. The optimization objective function of SVM classifier is as follows:

$$\begin{aligned}
L(\mathbf{w}, \boldsymbol{\beta}, \mathbf{a}) &= \sum_{p=1}^n a_p - \frac{1}{2} \sum_{p,q=1}^n y_p y_q a_p a_q K \langle x_p, x_q \rangle \\
s.t. \left\{ \begin{array}{l} K \langle x_p, x_q \rangle = x_p^T x_q \\ \mathbf{w} = \sum_{p=1}^l a_p y_p x_p \\ \sum_{p=1}^l a_p y_p = 0 \\ 0 \leq a_p \leq C, p = 1, \dots, n \end{array} \right. & \quad (14)
\end{aligned}$$

where L is the Lagrange function, \mathbf{w} is the normal vector of the fitted hyperplane, $\boldsymbol{\beta}$ is the displacement term determining the distance between the fitted hyperplane and the origin, and \mathbf{a} is the fitting error, $K \langle x_p, x_q \rangle$ is a linear kernel, \mathbf{x} is the value of BN features, $\mathbf{y} \in \{-1, +1\}$ represents labels, n is the number of training samples, p is the sample number in the training set, q is the sample number in the test set, and the parameter $C = 1$.

3. Results

A linear transformation transfers the original node features to a low-dimensional space. Equation (2) is used to refine the interaction weights, and the modified linear unit (Relu) is selected as its activation function. These interaction weights are normalized according to Eq (3) to construct an ADM, which guides the diffusion process to generate a joint node representation. Bilinear pooling is used to extract the connected features to build hypergraph, t -test is used to select the features, and SVM is used for classification. In the classification, the label of ESRDaMCI group is set to 1 and the label of normal group is set to -1. Because of the limited number of samples, leave-one-out cross-validation is adopted to evaluate the performance of HRMBN. In short, one is tested and the others are tested in the training model. The effects of different parameters on the classification performance of ESRDaMCI are discussed to determine the optimal parameters of HRMBN. It is compared with seven of the most advanced multimodal BN construction methods.

3.1. Parameter selection

The range of the number of nearest neighbors k is set as $[1, 20]$, and the range of the L_1 norm regularization parameter λ and the HMR parameter β are set as $[2^{-5}, 2^5]$. The significance level of t -test features is set to 0.05, and the linear kernel classifier parameter C is set to 1. Because the proposed model has multiple parameters, the grid search method cannot find the optimal parameters directly. The strategy of this study is to use leave-one-out cross-validation method to gradually calculate the optimal parameter values of the model, that is, first, the number of neighbors k is determined based on the hypergraph generated by the node representation and connection features, and then the regularization parameters λ and β are determined. The test results are averaged to measure the performance of the model. The model is repeatedly trained to determine the optimal hyperparameter, and the original samples are used to test the optimal hyperparameter model to avoid data leakage. Classification accuracy (ACC), area under ROC curve (AUC), sensitivity (SEN) and specificity (SPE) are used to evaluate the classification performance [37].

KNN algorithm is utilized to construct hypergraphs according to the generated node representation and connection features [38]. Specifically, we select k nearest vertices to generate hyperedges. As shown in Figure 2, $k = 1$ means that no hypergraph is formed. By comparing the values of various classification indexes between normal group and ESRDaMCI group under different k , it can be seen that when the value of k is 8, the best ACC is 86.6457%. When the value of k changes from small to large, the classification performance increases first and then decreases. The cause might be that for small values of k it describes features that are too dense. When the value of k is large, the hypergraph depicts the overall structural features of BN rather than local features, and many nodes on the hyperedge may belong to different categories, so it is difficult to well reflect the structural features of BN. If the hypergraph is not constructed (that is, when k value is 1) and the classification is performed directly, the effect is unsatisfactory, indicating that the hypergraph with moderate k value is helpful to improve the classification performance. This is basically consistent with the research conclusion of Shao et al. [34].

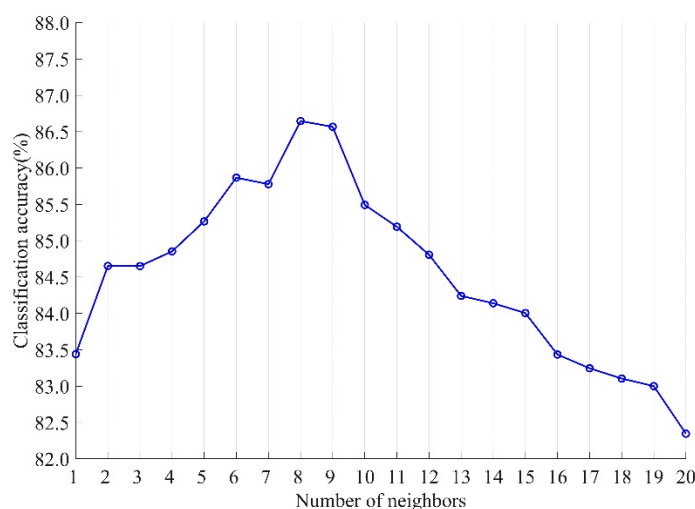


Figure 2. Classification accuracy of different nearest neighbors.

As the L_1 norm regular term is not derivable, the proximal operator method [38] is used to optimize and solve it. Firstly, the gradient descent method is used to update \mathbf{B}^t in Eq (13) m times, with a step of α_m . Then the nearest neighbor operator of the L_1 norm regularization term is computed to impose soft threshold operations on the elements in \mathbf{B}^t . After the completion of each gradient descent calculation, the nearest neighbor operator method is used to calculate \mathbf{B}^t 's nearest neighbor operator, and it is put into the next iteration for updating. So repeatedly, when the objective function in Eq (13) converges, the optimal solution of \mathbf{B}^t is obtained, that is, the HRMBN. The L_1 norm regularization term plays a role in removing redundant features and making the fused BN sparser. HMR term retains the discriminative information of each subject, so as to induce more discriminative features. In general, the regularization parameters λ and β are important to regulate the complexity of building the fused BN. Figure 3 shows the classification accuracy values of normal group and ESRDaMCI group with different regularization parameters.

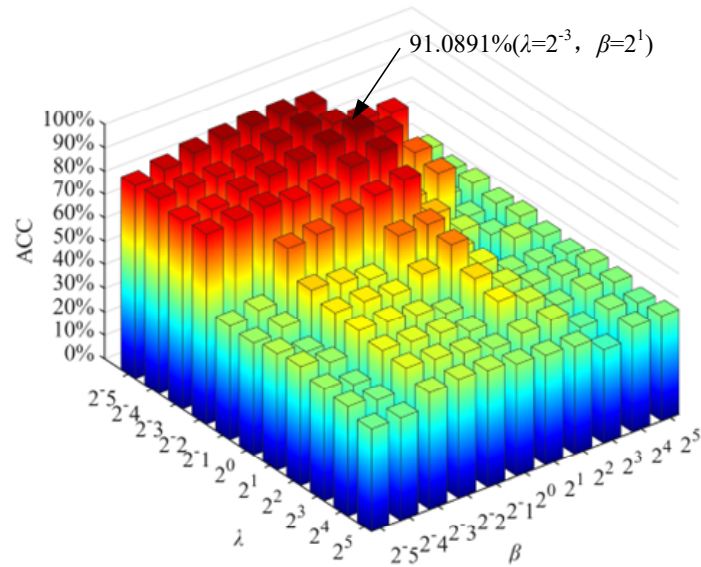


Figure 3. Classification accuracy of different regularization parameter combinations.

Since there is no parameter selection task involved in determining the regularization parameters, we calculated ACC based on the results of leave-one-out cross-validation for all subjects only. The final result is extremely sensitive to the regularization parameter, and the appropriate combination of the L_1 norm regularization parameter λ and the HMR parameter β can help to improve the classification performance. In particular, when $\lambda = 2^{-3}$ and $\beta = 2^1$, the best ACC (91.0891%) is achieved. As the values of λ and β change, especially when $\lambda \geq 2^{-1}$, ACC has an obvious downward trend. To sum up, the number of neighbors is set as 8, and the regularization parameter $\lambda = 2^{-3}$ and $\beta = 2^1$ are applied into construct the multimodal BN.

3.2. Contrast experiment

It is compared with two single-modal network methods and seven of the most advanced multimodal network methods to verify its effectiveness. In the unimodal method, FN matrix of DKI normalized by Minmax is used as the network and *Pearson's* correlation coefficient extracted from fMRI time series by *Pearson's* correlation is used as the network. Multi-model methods include multi-kernel [39], multi-linear principal component Analysis (MPCA) [40], kernelized Support Tensor Machine (KSTM) [41], Joint Structural Functional Connectivity (JFSC) [42], Multi-view Graph Convolutional Network (MVGCN) [43], Diffusion Convolutional Neural Network (DCNN) [44] and Attention Diffusion Bilinear Neural Network (ADBNN) [32]. According to the model inputs, the fusion methods of these multimodal fusion methods can be divided into two ways. Post-fusion (Multi-kernel, MPCA, KSTM) and pre-fusion (JFSC, MVGCN, DCNN, ADBNN). Post fusion is to fuses at the decision level. Pre-fusion to fuse the information of the two modes together by setting the model in the input stage. The method in this study belongs to pre-fusion. The above methods all use *t*-test method for feature selection and use linear kernel SVM classifier for classification. Their classification performance for ESRDaMCI is evaluated by leave-one-out cross-validation, as shown in Table 2. The optimal classification results are indicated in bold.

Table 2. Classification performance of different methods.

| Methods | ACC (%) | SEN (%) | SPE (%) | AUC |
|-------------------|-------------------------|-------------------------|-------------------------|------------------------|
| DKI (FN) | 69.8113 ± 4.2871 | 72.5490 ± 1.4290 | 53.8462 ± 2.5617 | 0.6953 ± 3.3493 |
| fMRI (PC) | 72.4314 ± 2.8581 | 71.4435 ± 3.1146 | 66.7949 ± 1.4570 | 0.7504 ± 3.4192 |
| Multi-kernel [39] | 73.5821 ± 5.7912 | 69.8234 ± 3.3247 | 75.4712 ± 2.6145 | 0.7231 ± 1.0767 |
| MPCA [40] | 67.5541 ± 1.5424 | 66.6715 ± 2.8952 | 79.1628 ± 5.4774 | 0.7671 ± 0.2130 |
| KSTM [41] | 70.0756 ± 3.1433 | 80.1643 ± 6.3478 | 61.5717 ± 3.3541 | 0.7982 ± 4.2041 |
| JSFC [42] | 63.4320 ± 3.5114 | 73.9417 ± 3.2264 | 60.6984 ± 2.6427 | 0.6864 ± 3.6714 |
| MVGCN [43] | 81.6488 ± 4.6481 | 86.8074 ± 1.4194 | 77.5132 ± 4.2438 | 0.8081 ± 4.0278 |
| DCNN [44] | 79.4045 ± 2.2725 | 74.1611 ± 0.5384 | 80.9744 ± 3.9925 | 0.7937 ± 0.8421 |
| ADBNN [32] | 86.7439 ± 1.4567 | 82.7921 ± 4.5711 | 84.7233 ± 3.7440 | 0.8874 ± 2.1534 |
| HRMBN | 91.0891 ± 2.5417 | 86.6461 ± 2.8941 | 89.7436 ± 2.1513 | 0.9023 ± 1.1164 |

Obviously, our method outperforms other methods for ESRDaMCI except SEN, and achieves the best classification effect. The best ACC, SPE and AUC are 91.0891% ± 2.5417%, 89.7436% ± 2.1513% and 0.9023 ± 1.1164, respectively. Compared with other methods, the error range of the proposed method is smaller, indicating that HRMBN is more stable and the classification performance is better. Compared with the suboptimal ADBNN method, the average ACC, SEN, SPE and AUC are improved by 4.3452, 3.8540, 5.0203 and 0.0149, respectively. In addition, it is found that most of the classification tasks using multimodality-based methods performed better than the single modality methods using only fMRI or DKI. This validates that combining two types of brain connections can provide complementary information and thus improve classification performance. For example, the accuracy of multi-kernel using simple combination strategy is at least 1.1507% higher than that of fMRI only method. Although JSFC combines fMRI and DKI, the accuracy obtained by JSFC is lower than that obtained by fMRI-based methods. This result may be due to the fact that most fMRI information does not involve the SC reconstruction process.

3.3. Discriminative brain regions

In this study, the connection in BN is used as a characteristic to identify patients with ESRDaMCI. Multimodal BN hypergraph representation is constructed based on the best classification performance, and then features with significant differences are selected ($p < 0.05$) to find some biomarkers for ESRDaMCI diagnosis. We calculate the number of brain regions involved in these connections and count the brain regions that appeared more frequently in the cross validation, and finally obtain 103 of the most discriminative features in the ESRDaMCI classification task. It is worth noting that there are 73 features selected from the brain functional network based on *Pearson's* correlation. It is clear that our HRMBN method has more discriminative features, and the generated network representation is better than traditional methods. Figure 4 shows the visualized discriminative features.

The thickness of each arc is inversely proportional to the corresponding p value, representing the discriminative power of the corresponding feature (not its actual connectivity strength). Since the brain regions selected in each cross validation are not the same, we count the top 15 brain regions most frequently selected in ESRDaMCI group and normal group classification as discriminative brain regions. From the connection in Figure 4, It can be seen that these brain regions are left middle frontal gyrus (Frontal_Mid_L), left middle frontal gyrus (Frontal_Mid_Orb_L), left inferior frontal gyrus

(Frontal_Inf_Orb_L), left central sulcus cover (Rolandic_Oper_L), and left supplementary motor area (Supp_Motor_Area_L), left medial superior frontal gyrus (Frontal_Sup_Medial_L), left gyrus rectus muscle (Rectus_L), right hippocampus (Hippocampus_R), left superior occipital gyrus (Occipital_Sup_L), left middle occipital gyrus (Occipital_Mid_L), left Occipital gyrus (Occipital_Inf_L), right occipital gyrus (Occipital_Inf_R), left angular gyrus (Angular_L), left middle temporal gyrus (Temporal_Mid_L), right temporal pole: middle temporal gyrus (Temporal_Pole_Mid_R). Map to the ICBM152 template space using BrainNet Viewer toolbox, as shown in Figure 5.

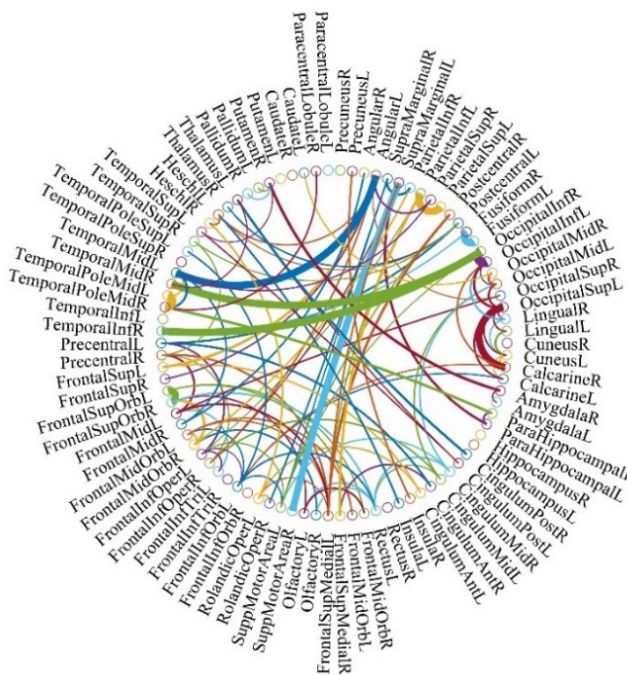


Figure 4. Discriminative features (connections).

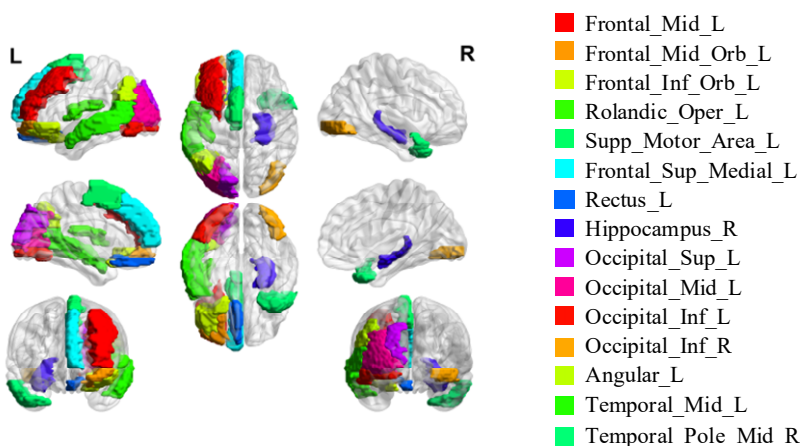


Figure 5. Discriminative brain regions.

Most of the selected brain regions, such as left middle temporal gyrus (Temporal_Mid_L), right hippocampus (Hippocampus_R), and right temporal pole: middle temporal gyrus (Temporal_Pole_Mid_R), are consistent with those brain regions with significant differences in topological attributes between the ESRD patients and the normal people in the previous study of Wu et al. [45]. The discriminative brain regions selected are mainly in the left side of the brain, which is thought to be involved in logical task processing, language and analytical thinking. For example, the left middle frontal gyrus (Frontal_Mid_L) in the frontal lobe, the left middle frontal gyrus (Frontal_Mid_Orb_L), the left inferior frontal gyrus (Frontal_Inf_Orb_L), the left medial superior frontal gyrus (Frontal_Sup_Medial_L), etc. [46], Mainly related to creative and advanced spiritual activities such as thinking and consciousness; The right hippocampus (Hippocampus_R) [47] plays a significant role in helping human short-term memory, long-term memory and spatial orientation; The left supplementary motor area (Supp_Motor_Area_L) [48] is mainly related to the voluntary motor control of trunk muscles. The left angular gyrus (Angular_L) is the visual language center (reading center). After the injury, people who have been able to read become unable to read (unable to understand the meaning of the copied words), although their vision are not affected. Occipital lobe includes left superior occipital gyrus (Occipital_Sup_L), left middle occipital gyrus (Occipital_Mid_L), left inferior occipital gyrus (Occipital_Inf_L) and right inferior occipital gyrus (Occipital_Inf_R) [49], which are responsible for vision, image recognition and image perception. left middle temporal gyrus (Temporal_Mid_L) and right temporal pole: middle temporal gyrus (Temporal_Pole_Mid_R) [50] are closely related to short-term memory, balance and emotion, etc. If these brain regions are damaged, personality changes will be caused. The multimodal BN hypergraph representation method can also identify the left rectus gyrus muscle (Rectus_L) region located on the orbital surface of the frontal lobe. Wee et al. [51] showed that morphological changes in the rectus muscle would affect the progression of MCI. These brain regions are selected, indicating that ESRDaMCI group had changes in memory, language, spatial visual processing and other aspects compared with normal group.

Some of the selected discriminative brain regions, including the right hippocampus (Hippocampus_R) and the left angular gyrus (Angular_L), belonging to the default mode network (DMN), are related to memory and visual language, respectively. DMN plays a key role in cognitive function and neuro-regulation. These results indicate that our study may provide the most discriminative features and brain regions that cause ESRDaMCI, and provide a reference for clinical diagnosis.

4. Discussion

In recent years, more and more attention has been paid to the study of some diseases associated with MCI. The borderline of such concomitant diseases remains a challenge. As the development of new neuroimaging techniques and the introduction of new research methods, these challenges may turn into opportunities for further insight into human brains. To date, there are relatively few focuses on ESRDaMCI classification. Most studies of BN depend on the properties of the unimodal data itself and only consider the pairwise relationship between brain regions, without taking into account the complementary information of FC and SC. In this study, a hypergraph representation method of multimodal BN is proposed to integrate FC and SC to construct BN, and it is applied to the classification of ESRDaMCI. Compared with the general network, this method naturally links the structural network and the functional network, and provides more feature information.

Current studies have shown that compared with only using a single mode, better classification accuracy can be obtained by fusing information from multiple modes [52]. The biggest difference between multimodal BN analysis and traditional multimodal data analysis lies in the natural connection between structural network and functional network. Structure can often affect function, so the correlation information between two modes can be further explored. Previous studies have modeled multimodal fusion. Mišić et al. [53] analyzed the connection between the two by partial least squares method, and found a number of closely related sub-networks and important nodes. Goñi et al. [54] directly used the connecting edge strength of SC to predict FC and found that there was a high degree of consistency in some brain regions. Nevertheless, these methods do not consider how to integrate two modes of information, but directly use the single mode data itself to directly fuse. Therefore, how to describe the correlation information between brain regions is very important. The method in this study automatically learns node interaction from FC and SC instead of using SC directly. The hypergraph constructed according to the generated node representation and connection features, whose multiple vertices are on the same hyperedge, can well reflect this potential correlation information.

It is worth mentioning that we generate a joint node representation of FC and SC by using diffusion processes, rather than simply treating them as two patterns to be spliced together as in the existing methods. FC and SC are also integrated in ADM which guides the diffusion process. In the map, the connections of nodes are determined by SC, and the connection weights between nodes are learned based on FC. The direct and indirect connections (that is, the diffusion step and two step diffusion) do not share each step of the parameters. For that reason, multi-step diffusion helps to increase the risk of excessive fitting. The HMR and the regularization term of L_1 norm are introduced to increase the prior information appropriately, so as to reduce the complexity of the model, enhance the robustness and prevent overfitting. Moreover, unlike the traditional approach of representing node interactions using non-directed joins, our approach learns directed node interactions. As seen from ADM constructed by Eqs (2) and (3), the directed node interactions contain weight information and direction information. The directional information of this diffusion map is exactly similar to the effective connections describing effective interactions between brain regions. Experimental results in Table 2 verify that the proposed method performs better than the traditional combination method.

However, there are some improvements in the proposed method. The multi-head attention mechanism will be explored and integrated into our model. It is likely to help improve classification performance. Node representations are generated in the model using only the spatial attention mechanism. Given that fMRI data can represent time by measuring fluctuations, temporal information should also be taken into account during representation learning. For the next stage, we plan to explore how to joint temporal and spatial factors to characterize the temporal and spatial characteristics of BN [55]. Furthermore, the dataset in this study has a limited number of samples, so it is necessary to add more samples and then train diffusion through two steps and above to increase the range of interactions. The brain regions mentioned above are defined using the AAL template, and only 90 brain regions are selected to construct the BN. Several other available templates should be considered for dividing the brain into finer brain regions.

5. Conclusions

In this study, a hypergraph representation method of multimodal BN is proposed to construct BN (i.e., HRMBN) to identify patients with ESRDaMCI. This method effectively integrates FC and SC DKI and fMRI data into a learning framework, where the characteristics of network nodes are refined

based on automatic learning node graph. The second order statistics of the features of these nodes can be further extracted by bilinear pooling for classification, so as to better understand the potential correlation between brain function and structure, and provide a new method for brain analysis. The entire network is trained in an end-to-end manner and shows better performance on real ESRDaMCI datasets, with ACC, SEN, SPE and AUC reaching 91.0891, 86.6461, 89.7436% and 0.9023, respectively. In addition, the discriminative brain regions are identified according to the selected features to better reflect the pathogenesis of ESRDaMCI. The HRMBN method is effective in identifying ESRDaMCI with functional or structural abnormalities.

Acknowledgments

This work was supported by National Natural Science Foundation of China (grant No. 51877013), and Jiangsu Provincial Key Research and Development Program (grant No. BE2021636). This work was also sponsored by Qing Lan Project of Jiangsu Province.

Conflict of interest

The authors declare there is no conflict of interest.

References

1. S. M. Li, X. F. Ma, R. W. Huang, M. Li, J. Z. Tian, H. Wen, et al., Abnormal degree centrality in neurologically asymptomatic patients with end-stage renal disease: A resting-state fMRI study, *Clin. Neurophysiol.*, **127** (2016), 602–609. <https://doi.org/10.1016/j.clinph.2015.06.022>
2. X. F. Ma, G. H. Jiang, S. M. Li, J. H. Wang, W. F. Zhan, S. Q. Zeng, et al., Aberrant functional connectome in neurologically asymptomatic patients with end-stage renal disease, *PloS One*, **10** (2015), e0121085. <https://doi.org/10.1371/journal.pone.0121085>
3. E. O’Lone, M. Connors, P. Masson, S. Wu, P. J. Kelly, D. Gillespie, et al., Cognition in people with end-stage kidney disease treated with hemodialysis: A systematic review and Meta-analysis, *Am. J. Kidney Dis.*, **67** (2016), 925–935. <https://doi.org/10.1053/j.ajkd.2015.12.028>
4. K. Karunaratne, D. Taube, N. Khalil, R. Perry, P. A. Malhotra, Neurological complications of renal dialysis and transplantation, *Pract. Neurol.*, **18** (2018), 115–125. <https://doi.org/10.1136/practneurol-2017-001657>
5. S. H. Wang, Y. Zhang, Y. J. Li, W. J. Jia, F. Y. Liu, M. M. Yang, et al., Single slice based detection for Alzheimer’s disease via wavelet entropy and multilayer perceptron trained by biogeography-based optimization, *Multimed. Tools Appl.*, **77** (2018), 10393–10417. <https://doi.org/10.1007/s11042-016-4222-4>
6. S. H. Wang, Y. D. Zhang, G. Liu, P. Preetha, T. F. Yuan, Detection of Alzheimer’s disease by three-dimensional displacement field estimation in structural magnetic resonance imaging, *Int. J. Alzheimers Dis.*, **50** (2016), 233–248. <https://doi.org/10.3233/JAD-150848>
7. T. K. Chacko, H. Zhuang, K. Z. Nakhoda, B. Moussavian, A. Alavi, Applications of fluorodeoxyglucose positron emission tomography in the diagnosis of infection, *Nucl. Med. Commun.*, **24** (2003), 615–624. <https://doi.org/10.1097/00006231-200306000-00002>

8. X. L. Jiang, J. Q. Wen, L. J. Zhang, G. Zheng, X. Li, Z. Zhang, et al., Cerebral blood flow changes in hemodialysis and peritoneal dialysis patients: An arterial-spin labeling MR imaging, *Metab. Brain Dis.*, **31** (2016), 929–936. <https://doi.org/10.1007/s11011-016-9829-7>
9. L. Li, J. Y. Liu, F. X. Liang, H. D. Chen, R. G. Zhan, S. L. Zhao, et al., Altered brain function activity in patients with dysphagia after cerebral infarction: A resting-state functional magnetic resonance imaging study, *Front. Neurol.*, **13** (2022), 782732. <https://doi.org/10.3389/fneur.2022.782732>
10. R. Marta, A. Lukasz, M. Marek, Clinical application of diffusion tensor imaging and fiber tractography in the management of brainstem cavernous malformations: A systematic review, *Neurosurg. Rev.*, **45** (2022), 2027–2040. <https://doi.org/10.1007/s10143-022-01759-7>
11. J. X. Wang, S. C. Wu, Y. Sun, J. M. Lu, J. L. Zhang, Y. Fang, et al., Brain microstructural alterations in the left precuneus mediate the association between KIBRA polymorphism and working memory in healthy adults: A diffusion kurtosis imaging study, *Brain Imaging Behav.*, **2022** (2022), 1–10. <https://doi.org/10.1007/s11682-022-00703-z>
12. J. W. Dong, X. F. Ma, W. H. Lin, M. C. Liu, S. S. Fu, L. H. Yang, et al., Aberrant cortical thickness in neurologically asymptomatic patients with end-stage renal disease, *Neuropsychiatr. Dis. Treat.*, **14** (2018), 1929–1939. <https://doi.org/10.2147/NDT.S170106>
13. F. F. Udo, W. Dominik, S. Armin, F. Andreas, Altered whole-brain white matter networks in preclinical Alzheimer’s disease, *Neuroimage Clin.*, **8** (2015), 660–666. <https://doi.org/10.1016/j.nicl.2015.06.007>
14. Y. An, X. F. Ma, T. M. Lu, D. Zhang, Application of magnetic resonance imaging molecular probe in the treatment of cerebral infarction and paralysis of hind limbs with neural stem cells derived from pluripotent stem cells, *World Neurosurg.*, **138** (2020), 608–618. <https://doi.org/10.1016/j.wneu.2020.01.036>
15. W. B. Li, X. Wang, X. E. Wei, M. L. Wang, Susceptibility-weighted and diffusion kurtosis imaging to evaluate encephalomalacia with epilepsy after traumatic brain injury, *Ann. Clin. Transl. Neur.*, **5** (2018), 552–558. <https://doi.org/10.1002/acn3.552>
16. E. L. Pogosbekian, I. N. Pronin, N. E. Zakharova, A. I. Batalov, A. M. Turkin, T. A. Konakova, et al., Feasibility of generalised diffusion kurtosis imaging approach for brain glioma grading, *Neuroradiology*, **63** (2021), 1241–1251. <https://doi.org/10.1007/s00234-020-02613-7>
17. X. A. Bi, X. Hu, H. Wu, Y. Wang, Multimodal data analysis of Alzheimer’s disease based on clustering evolutionary random forest, *IEEE J. Biomed. Health Inf.*, **24** (2020), 2973–2983. <https://doi.org/10.1109/JBHI.2020.2973324>
18. Z. Q. Zhang, W. Liao, H. F. Chen, D. Mantini, J. R. Ding, Q. Xu, et al., Altered functional–structural coupling of large-scale brain networks in idiopathic generalized epilepsy, *Brain*, **134** (2011), 2912–2928. <https://doi.org/10.1093/brain/awr223>
19. M. E. Lynall, D. S. Bassett, R. Kerwin, P. J. McKenna, M. Kitzbichler, U. Muller, et al., Functional connectivity and brain networks in schizophrenia, *J. Neurosci.*, **30** (2010), 9477–9487. <https://doi.org/10.1523/JNEUROSCI.0333-10.2010>
20. Y. D. Zhang, S. H. Wang, Y. X. Sui, M. Yang, B. Liu, H. Cheng, et al., Multivariate approach for Alzheimer’s disease detection using stationary Wavelet entropy and predator-prey particle swarm optimization, *J. Alzheimer’s Dis.*, **65** (2018), 855–869. <https://doi.org/10.3233/JAD-170069>
21. C. Peng, T. Y. Luo, H. Yang, Immediate abnormal intrinsic brain activity patterns in patients with end-stage renal disease during a single dialysis session: A resting-state functional MR imaging study, *Chin. Imaging Soc. Integr. Med.*, **2** (2019), 17025. <https://doi.org/10.26914/c.cnkihy.2019.017025>

22. M. Wang, J. Huang, M. Liu, D. Zhang, Functional connectivity network analysis with discriminative hub detection for brain disease identification, in *Proceedings of the AAAI Conference on Artificial Intelligence*, **33** (2019), 1198–1205. <https://doi.org/10.1609/aaai.v33i01.33011198>
23. C. Y. Wee, P. T. Yap, K. Denny, J. N. Browndyke, G. G. Potter, K. A. Welsh-Bohmer, et al., Resting-state multi-spectrum functional connectivity networks for identification of MCI patients, *PloS One*, **7** (2012), e37828. <https://doi.org/10.1371/journal.pone.0037828>
24. J. Yu, Y. Rui, Y. Y. Tang, High-order distance-based multi-view stochastic learning in image classification, *IEEE Trans. Cybern.*, **44** (2014), 2431–2442. <https://doi.org/10.1109/TCYB.2014.2307862>
25. Y. X. Ji, Y. T. Zhang, H. F. Shi, Z. Q. Jiao, S. H. Wang, C. Wang, Constructing dynamic brain functional networks via hyper-graph manifold regularization for mild cognitive impairment classification, *Front. Neurosci.*, **15** (2021), 669345. <https://doi.org/10.3389/fnins.2021.669345>
26. R. I. Kondor, J. Lafferty, Diffusion kernels on graphs and other discrete structures, in *Proceedings of the 19th International Conference on Machine Learning*, (2002), 315–322.
27. J. B. Pereira, D. Van Westen, E. Stomrud, T. O. Strandberg, G. Volpe, E. Westman, et al., Abnormal structural brain connectome in individuals with preclinical Alzheimer’s disease, *Cereb. Cortex*, **28** (2017), 3638–3649. <https://doi.org/10.1093/cercor/bhx236>
28. C. Y. Xu, C. C. Chen, Q. W. Guo, Y. W. Lin, X. Y. Meng, G. Z. Qiu, et al., Comparative study of MOCA-B and MES in the recognition of amnesic mild cognitive impairment, *J. Alzheimer’s Dis.*, **4** (2021), 33–36. <https://doi.org/10.3969/j.issn.2096-5516.2021.01.005>
29. Z. X. Cui, S. Y. Zhong, P. F. Xu, Y. He, G. L. Gong, PANDA: A pipeline toolbox for analyzing brain diffusion images, *Front. Hum. Neurosci.*, **7** (2013), 42. <https://doi.org/10.3389/fnhum.2013.00042>
30. R. Mikail, S. Olaf, Complex network measures of brain connectivity: Uses and interpretations, *Neuroimage*, **52** (2010), 1059–1069. <https://doi.org/10.1016/j.neuroimage.2009.10.003>
31. K. Li, L. J. Liu, Q. Yin, W. H. Dun, X. L. Xu, J. X. Liu, et al., Abnormal rich club organization and impaired correlation between structural and functional connectivity in migraine sufferers, *Brain Imaging Behav.*, **11** (2017), 526–540. <https://doi.org/10.1007/s11682-016-9533-6>
32. J. S. Huang, L. P. Zhou, L. Wang, D. Q. Zhang, Attention-diffusion-bilinear neural network for brain network analysis, *IEEE Trans. Med. Imaging*, **39** (2020), 2541–2552. <https://doi.org/10.1109/TMI.2020.2973650>
33. T. Lin, A. RoyChowdhury, S. Maji, Bilinear CNN models for finegrained visual recognition, in *Proceedings of the IEEE International Conference on Computer Vision*, (2015), 1449–1457. <https://doi.org/10.48550/arXiv.1504.07889>
34. W. Shao, Y. Peng, C. Zu, M. L. Wang, D. Q. Zhang, Hypergraph based multi-task feature selection for multimodal classification of Alzheimer’s disease, *Comput. Med. Imaging Graphics*, **80** (2019), 101663. <https://doi.org/10.1016/j.compmedimag.2019.101663>
35. S. Huang, J. Li, L. Sun, J. Liu, T. Wu, K. Chen, Learning brain connectivity of Alzheimer’s disease from neuroimaging data, in *Advances in Neural Information Processing Systems 22 (NIPS 2009)*, (2009), 808–816.
36. X. M. Liu, J. S. Tang, Mass classification in mammograms using selected geometry and texture features and a new SVM-based feature selection method, *IEEE Syst. J.*, **8** (2014), 910–920. <https://doi.org/10.1109/JSYST.2013.2286539>

37. Y. Li, J. Liu, X. Gao, B. Jie, M. Kim, P. T. Yap, et al., Multimodal hyper-connectivity of functional networks using functionally-weighted LASSO for MCI classification, *Med. Image Anal.*, **52** (2018), 80–96. <https://doi.org/10.1016/j.media.2018.11.006>
38. W. K. Li, X. W. Xu, W. Jiang, P. J. Wang, X. Gao, Functional connectivity network estimation with an inter-similarity prior for mild cognitive impairment classification, *Aging*, **12** (2020), 17328–17342. <https://doi.org/10.18632/aging.103719>
39. M. Dyrba, M. Grothe, T. Kirste, S. J. Teipel, Multimodal analysis of functional and structural disconnection in Alzheimer’s disease using multiple kernel SVM, *Hum. Brain Mapp.*, **36** (2015), 2118–2131. <https://doi.org/10.1002/hbm.22759>
40. H. P. Lu, N. P. Konstantinos, A. N. Venetsanopoulos, MPCA: Multilinear principal component analysis of tensor objects, *IEEE Trans. Neural Networks*, **19** (2008), 18–39. <https://doi.org/10.1109/TNN.2007.901277>
41. C. Chen, K. Batselier, W. J. Yu, N. Wong, Kernelized support tensor train machines, *Pattern Recognit.*, **122** (2022), 108337. <https://doi.org/10.1016/j.patcog.2021.108337>
42. S. H. Chu, K. K. Parhi, C. Lenglet, Function-specific and enhanced brain structural connectivity mapping via joint modeling of diffusion and functional MRI, *Sci. Rep.*, **8** (2018), 4741. <https://doi.org/10.1038/s41598-018-23051-9>
43. X. Zhang, L. F. He, K. Chen, Y. Luo, J. Y. Zhou, F. Wang, Multiview graph convolutional network and its applications on neuroimage analysis for Parkinson’s disease, in *AMIA Annual Symposium Proceedings*, (2018), 1147.
44. J. Atwood, D. Towsley, Diffusion-convolutional neural networks, in *Advances in Neural Information Processing Systems 29 (NIPS 2016)*, (2016), 1993–2001.
45. B. L. Wu, Z. Yue, X. K. Li, L. Li, M. Zhang, J. P. Ren, et al., Changes of brain functional network and its correlation with cognitive function in patients with end-stage renal disease, *Chin. J. Neuromed.*, **2** (2020), 181–187. <https://doi.org/10.3760/cma.j.issn.1671-8925.2020.02.012>
46. Y. D. Zhang, S. H. Wang, P. Preetha, J. Q. Yang, T. F. Yuan, Three-dimensional eigenbrain for the detection of subjects and brain regions related with Alzheimer’s disease, *J. Alzheimer’s Dis.*, **50** (2016), 1163–1179. <https://doi.org/10.3233/JAD-150988>
47. S. H. Wang, Y. D. Zhang, G. Liu, P. Preetha, T. F. Yuan, Detection of Alzheimer’s disease by three-dimensional displacement field estimation in structural magnetic resonance imaging, *J. Alzheimer’s Dis.*, **50** (2016), 233–248. <https://doi.org/10.3233/JAD-150848>
48. Y. D. Zhang, S. H. Wang, P. Preetha, Z. C. Dong, G. L. Ji, J. Q. Yang, Detection of Alzheimer’s disease and mild cognitive impairment based on structural volumetric MR images using 3D-DWT and WTA-KSVM trained by PSOTVAC, *Biomed. Signal Process.*, **21** (2015), 58–73. <https://doi.org/10.1016/j.bspc.2015.05.014>
49. S. H. Wang, S. D. Du, Y. Zhang, P. Preetha, L. N. Wu, X. Q. Chen, et al., Alzheimer’s disease detection by Pseudo Zernike moment and linear regression classification, *CNS Neurol. Disord. Drug Targets*, **16** (2017), 11–15. <https://doi.org/10.2174/1871527315666161111123024>
50. Y. D. Zhang, Z. C. Dong, P. Preetha, S. H. Wang, G. L. Ji, J. Q. Yang, et al., Detection of subjects and brain regions related to Alzheimer’s disease using 3D MRI scans based on eigen brain and machine learning, *Front. Comput. Neurosc.*, **9** (2015), 66. <https://doi.org/10.3389/fncom.2015.00066>

51. C. Y. Wee, P. T. Yap, W. Li, K. Denny, J. N. Browndyke, G. G. Potter, et al, Enriched white matter connectivity networks for accurate identification of MCI patients, *NeuroImage*, **54** (2011), 1812–1822. <https://doi.org/10.1016/j.neuroimage.2010.10.026>
52. D. Q. Zhang, Y. P. Wang, L. P. Zhou, H. Yuan, D. G. Shen, Multimodal classification of Alzheimer’s disease and mild cognitive impairment, *Neuroimage*, **55** (2011), 856–867. <https://doi.org/10.1016/j.neuroimage.2011.01.008>
53. B. Mišić, R. F. Betzel, M. A. De Reus, M. P. Van Den Heuvel, M. G. Berman, A. R. McIntosh, et al., Network-level structure-function relationships in human neocortex, *Cereb. Cortex*, **26** (2016), 3285–3296. <https://doi.org/10.1093/cercor/bhw089>
54. J. Goñi, M. P. Van Den Heuvel, A. Avena-Koenigsberger, N. Velez de Mendizabal, R. F. Betzel, A. Griffa, et al., Resting-brain functional connectivity predicted by analytic measures of network communication, *Proc. Natl. Acad. Sci.*, **111** (2014), 833–838. <https://doi.org/10.1073/pnas.1315529111>
55. X. Hua, J. G. Han, C. Zhao, H. P. Tang, Z. He, Q. H. Chen, et al., A novel method for ECG signal classification via one-dimensional convolutional neural network, *Multimedia Syst.*, **28** (2022), 1387–1399. <https://doi.org/10.1007/s00530-020-00713-1>



AIMS Press

©2023 the Author(s), licensee AIMS Press. This is an open access article distributed under the terms of the Creative Commons Attribution License (<http://creativecommons.org/licenses/by/4.0>)